Heliyon 11 (2025) e42800

Contents lists available at ScienceDirect

Heliyon

journal homepage: www.cell.com/heliyon

Research article

Pyrolysis kinetics, mechanism and thermodynamics of peanut shell based on Gaussian function deconvolution

Jialiu Lei [a,b,*], Liu Yang [a], Yuhao Wang [a], Dongnan Zhao [a]

[a] School of Materials Science and Engineering, Hubei Polytechnic University, Huangshi 435003, China
[b] The State Key Laboratory of Refractories & Metallurgy, Wuhan University of Science and Technology, Wuhan 430081, China

ARTICLE INFO

Keywords:
Pyrolysis kinetics
Pyrolysis mechanism
Thermodynamic analysis
Peanut shell
Gaussian function

ABSTRACT

As a typical biomass resource, peanut shell has the potential to produce energy and value-added products, as it is generated abundantly worldwide. Pyrolysis is increasingly utilized for the disposal of biomass wastes through thermal conversion into chemical raw materials. Assessing the pyrolysis kinetics, reaction mechanism, thermodynamic parameters for individual components of peanut shells is crucial for its valorization. In this study, conditions for pyrolysis were optimized under pure N_2 flow across temperatures ranging from 303 K to 1173 K at the temperature ramp of 10 K/min, 20 K/min, and 30 K/min. The peak-differentiating analysis using Gaussian function was employed to segregate the pyrolysis of peanut shell into several independent one-step parallel reactions, corresponding to pseudo-lignin, pseudo-cellulose, and pseudo-hemicellulose decomposition. The Coats–Redfern, Kissinger–Akahira–Sunose, Flynn–Wall–Ozawa, and Vyazovkin techniques were employed to estimate kinetic parameters and reaction mechanism for each pseudo-component of peanut shell. The performed analyses revealed that the average activation energy values generally followed an order of pseudo-lignin > pseudo-hemicellulose > pseudo-cellulose, with values of 174.31 kJ/mol, 133.89 kJ/mol, and 115.44 kJ/mol by Kissinger–Akahira–Sunose, 177.79 kJ/mol, 136.53 kJ/mol, and 120.33 kJ/mol by Flynn–Wall–Ozawa, and 174.96 kJ/mol, 134.29 kJ/mol, and 116.61 kJ/mol by Vyazoykin, respectively. The Coats–Redfern method indicated that the suitable mechanism of reaction for pseudo-hemicellulose and pseudo-cellulose were random nucleation-based, while diffusional-based mechanism was identified for pseudo-lignin. The thermodynamic analysis revealed that the decomposition of peanut shell was endothermic and non-spontaneous, and it can be converted into value-added sources of energy steadily through pyrolysis process. This study offers a reliable approximation of experimental data irrespective of pyrolysis behavior and guides the resourceful utilization of peanut shell.

1. Introduction

Given the rapid advancement of human society, the escalating global energy demand has resulted in a gradual depletion of energy resources and environmental degradation. The advancement of renewable energy sources and the enhancement of energy efficiency are feasible schemes to resolve these issues. In this context, biomass has attracted numerous scholars worldwide due to its widespread distribution, productivity, carbon neutrality, and potential contribution to fulfilling the objectives outlined in the Paris Agreement [1,

* Corresponding author. School of Materials Science and Engineering, Hubei Polytechnic University, Huangshi 435003, China.
E-mail address: leijialiu@hbpu.edu.cn (J. Lei).

https://doi.org/10.1016/j.heliyon.2025.e42800
Received 20 March 2024; Received in revised form 13 February 2025; Accepted 18 February 2025
Available online 19 February 2025

2]. Biomass typically encompasses various plants, animal byproducts, and derivatives thereof, with the biomass encountered in daily life predominantly originating from forestry, agriculture, and industrial waste [3]. Despite containing substantial energy reserves and boasting extensive output approximately 1.0×10^{11} tons annually worldwide, while the current utilization efficiency of biomass remains relatively low. Consequently, significant quantities of agricultural and forestry residues are either incinerated or discarded, leading to resource wastage and environmental pollution [4].

As the world's largest peanut producer, China accounts for more than 40 % of the world's total peanut production, and peanut shells account for about 30 % of the total mass of peanut producer. According to statistics, China's annual production of peanut shells up to 1.8×10^6 t [5], some of which were used as fuel fertilizer, feed, and fuel, while most of them were piled up or directly incinerated, resulting in a serious waste of resources. As a typical biomass resource, peanut shells have the potential to produce energy and value-added products, such as liquid (bio-oil), solid (biochar), gases (CO, CO_2, CH_4, H_2, light hydrocarbons) and so on by thermochemical conversion, and thus can contribute in the country's energy security protection and be helpful to the goal of achieving carbon neutrality before 2060 for national sustainable development. As a feedstock, peanut shells can be concentrated into pellets with increase mechanical density and strength facilitating subsequent use procedures. Therefore, the comprehensive beneficial value of peanut shell has been widely concerned.

Pyrolysis serves as a significant alternative for managing solid biomass waste within a thermochemical framework, yielding various valuable products [6–8]. It includes the high-temperature thermal breakdown of biomass under an inert atmosphere, leading to the formation of three primary products: bio-oil/tar, bio-char, and gas [9–11]. Additionally, pyrolysis facilitates thermal conversion and serves as a precursor to gasification or combustion processes. Over the past decades, extensive research has focused on enhancing our understanding of biomass pyrolysis behavior. Given the importance of kinetics parameters and reaction mechanisms in exploring the pyrolysis process, investigating biomass pyrolysis kinetics and mechanisms is crucial for describing practical conversion processes and optimizing reactor design [12,13]. In this sense, non-isothermal pyrolysis experiments carried outusing thermogravimetric analyzers have been widely used at lower heating rates. While for bubbling fluidized bed reactor, due to its high thermal inertia and fast heating rates, allowing the pyrolysis of biomass under isothermal conditions [14].

Reviewing the literature reveals that numerous investigations have been carried out in this area using various model-free and model-fitting methods [15–18]. The model-free method were commonly recommended in kinetic analysis over a wide range of conversion without knowledge about the actual reaction model at different ramping rates [19,20]. Additionally, the Coats–Redfern (CR) model-fitting method was usually used for the estimation of reaction mechanism and kinetic triplet based on the assumed reaction mechanism and the kinetic triplets were independent of the ramping rate [21,22]. Therefore, model-free methods were commonly used in kinetic analysis, such as Flynn–Wall–Ozaw (FWO), Kissinger–Akahira–Sunose (KAS), and Vyazoykin methods, and was found to be more accurate and reliable for assessment of kinetic parameters of the biomass pyrolysis compared to model-fitting methods [23,24]. While traditional integral model-free methods may result in determination activation energy as a conversion function [25]. The integral model-free methods require lower heating rates to ensure efficient homogeneous decomposition. Ghodke [26] and Bhavanam [27] applied the distributed activation energy models (DAEM) to determine the kinetic parameters for peanut shell pyrolysis. Torres-García [28] investigated the thermo-kineticstudy of peanut shell and used Kissinger, KAS, Friedman methods to determine the activation energy. Varma [29] explored the pyrolysis kinetic parameters and thermodynamic parameters by FWO, Kissinger, KAS and CR methods. Kumar [30] yielded activation energy for peanut shell pyrolysis using the iso-conversional methods of FWO, KAS, Starink, Tang, and Vyazovkin. These studies on peanut shell pyrolysis behavior mainly focus on the application of model-free models to analyze the activation energy in entire process, and few studies on the mechanism function of peanut shell pyrolysis. However, due to the intricate nature of biomass pyrolysis, a single reaction model or mechanism cannot adequately characterize the entire process. Studies demonstrate that biomass primarily comprises hemicellulose, cellulose, and lignin, with hemicellulose degradation initiating first during temperature ramping, followed by cellulose, before eventually completing, while lignin degradation occurs throughout the process [31–33]. Nevertheless, by dividing the pyrolysis process into several independent one-step parallel reactions and determining the kinetics, thermodynamics, and mechanism of these parallel reactions, insights into the pyrolysis behaviors of the overall pyrolysis process can be gleaned.

Recently, the deconvolution technique has emerged as a recommended approach for analyzing simultaneous reaction kinetics, particularly in the context of biomass. This technique allows for the separation of reaction rates into three primary components within biomass. Subsequently, for each distinct reaction peak, both model-free and model-fitting techniques can be appropriately applied. Yang Wang et al. utilized a three-parallel Gaussian reaction model to describe the pyrolysis process of tobacco straw, and provided better results of kinetic parameters, thermodynamic parameters, and reaction mechanism models [34]. Runzhou Huang et al. reported the thermal decomposition kinetics of nature fibers by handling deconvolution with Gaussian function, the activation energy of the heartwood and sapwood were calculated, and the results obtained by the various methods were compared [35]. Bojan Janković et al. applied the Gaussian multi-peak fitting and peak-to-peak methods investigated the kinetic of five different biomasses, and the results of kinetic model and their interpretation were presented [36]. Shuai Guo et al. explored the combustion behavior of fungus bran biofuel of each component using Gaussian deconvolution fitting, and multicomponent combustion kinetics were revealed [37]. Ruiyu Chen et al. investigated the pyrolysis mechanism and kinetics of industrial nontyre rubber wastes using peak-differentiating analysis with Guassian function, and judged that Guassian function is suitable to well separate the pyrolysis of overlapping components into six independent one-step parallel reactions [38]. These available literatures shown that Guassian function gave an appropriate deconvolution for the kinetic model of bimass pyrolysis.

Hence, this study employs peak-differentiating analysis using Gaussian functions to segregate the pyrolysis of peanut shell into three independent one-step parallel reactions. Through the deconvolution technique, the rates of reactions are parsed into P-Lig, P-Cell, and P-Hem. The deconvolved profiles of these pseudo-components (P-Com) can then be analyzed usingmodel-free models of

FWO,KAS, and Vyazoykin, and CR model-fitting method, and then the pyrolysis kinetics, thermodynamics, and mechanism of peanut shellare revealed and discussed. These findings providesan in-depth insight into the pyrolysis mechanism of peanut shell, benefiting scientific agricultural biomass utilization.

2. Materials and methods

2.1. Materials

The peanut shells were sourced from Hubei provinceand dried at 373 K for 10 h to eliminate moisture content before being pulverized. Following this, the samples were finely ground and sieved to achieve uniformity and a small particle size, passing through a 150-mesh screen. The particle size range ranging from 80 to 106 μm was selected based on the recommendations of Van de Velden [39] and Brems [40] to minimizethe mass transfer and heat transfer limitations. The bulk density of the samples were 0.7 g/cm^3, and the finely ground samples were then sealed in plastic bags and stored under vacuum conditions before classification and thermogravimetric procedures.

2.2. Physiochemical analyses

2.2.1. Proximate and ultimate analyses

The proximate analysis of peanut shells was conducted in accordance with the GB/T212–2008 standard. The moisture content was measured by heating drying bamboo at 378 K for 24 h. The dried bamboo was then heated to 1173 ± 10 K for 7 min to assess the volatiles. The ash content was obtained by heating dry biomass at 1123 ± 10 K until a constant mass was achieved, and the fixed carbon content was obtained from the difference. For the ultimate analysis, a CHNS/O analyzer (Vario Micro cube, Elementar, Germany) was utilized. This analyzer allowed for the simultaneous detection of weight percentages of C, H, N, and S within samples, with the weight percentage of O determined by difference. Each experiment was repeated at least twice, and average values were reported.

The composition of the peanut shell is presented in Table 1. The high volatile and fixed carbon content in the peanut shell highlights its potential as a fuel source for thermochemical processes. It is worth noting that the low nitrogen and sulfur content are advantageous as they contribute to lower toxic NOx and SOx emissions during conversion processes, thereby positioning the peanut shell as a promising alternative for bioenergy production concerning environmental sustainability and high volatility.

2.2.2. FTIR analysis

To explore the functional groups present in the peanut shell, the Fourier Transform Infrared (FTIR) analysis was conducted via the KBr method and the results are presented in Fig. 1. The experiments were conducted in quadruplicate from 400 to 4000 cm^{-1}.

The corresponding wave number and atomic bonds of the functional groups were listed in Table 2. The broad absorption peak observed at 3414 cm^{-1} originates from O–H stretching vibrations, reflecting the presence of phenolic, alcoholic, and carboxylic groups. The peaks at 2924 cm^{-1} stem from C–H stretching vibrations, demonstrating the presence of alkanes and alkyl groups. Moreover, C=O stretching vibration at 1730 cm^{-1} confirms the existence of carboxylic acids, aldehydes, andketones groups, associated with hemicelluloses [41]. The absorbance peak at 1648 cm^{-1} indicates C=C stretching vibrations, suggesting the presence of aromatic groups attributed to cellulose and lignin in the peanut shell [42]. The band observed at 1233 cm^{-1} is due to the stretching of COOH in carboxylic acids and esters groups of the hemicellulose component, while the band at 1096 cm^{-1} originates from C–O stretching vibrations, likely related to the effects of alcohols, esters, and ethers groups found in cellulose and lignin [43].

2.2.3. XRD analysis

The crystallographic composition of the peanut shell was assessed using X-ray diffraction (XRD) (Model SmartLab system, Japan), as shown in Fig. 2. The XRD analysis covered an angle 2θ range from 10° to 80°, with a scanning speed of 5°/min and CuKα radiation at 40 kV and 30 mA. Two prominent diffraction peaks at approximately 16° and 22° were observed, originating from the reflection of 101 and 002 planes [44], respectively. These peaks are attributed to the presence of semi-crystalline cellulose components.

2.2.4. SEM analysis

Field emission scanning electron microscopy (FESEM) was employed to explore the microstructure of peanut shells. Fig. 3 reveals that the peanut shell exhibits an irregular rod-like shape. The surfaces of the particles appear highly rough and turbid, devoid of surface pores. Additionally, nano adsorption particles are visible on the surface, and distinct fiber characteristics are apparent.

Table 1
Proximate analysis and ultimate analysis of peanut shell.

Proximate analysis/%				Ultimate analysis/%				
Moisture	Ash	Volatiles	Fixed carbon	N	C	H	S	O
8.16	20.26	57.20	14.38	0.54	34.97	5.33	0.01	59.69

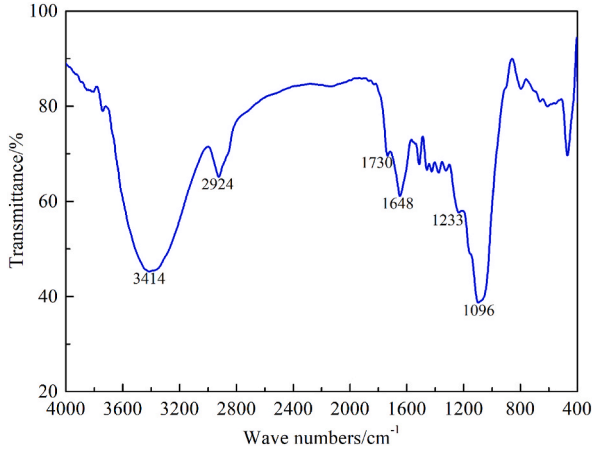

Fig. 1. FTIR spectrum of the peanut shell.

Table 2
FTIR spectrum peaks bands related to peanut shell.

Wave number cm^{-1}	Band position cm^{-1}	Vibration	Functional group	Biomass component
3200–3600	3414	O–H stretching	Phenolics, alcoholics, carboxylics	
2800–3000	2924	C–H stretching	Alkanes, alkyls	
1690–1750	1730	C=O stretching	Carboxylic acids, aldehydes,ketones	Hemicellulose
1570–1690	1648	C=C stretching	Aromatics	Cellulose, lignin
1200–1250	1233	COOH stretching	Carboxylic acids, esters	Hemicellulose
1000–1200	1096	C–O stretching	Alcohols, esters, ethers	Cellulose, lignin

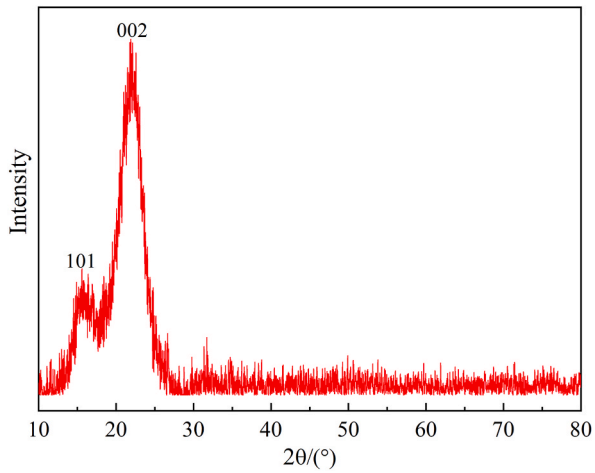

Fig. 2. XRD pattern analysis of peanut shell.

2.3. Deconvolution technique

In the present study, peak-differentiating analysis utilizing Gaussian functions is applied to the thermogram curves to segregate the pyrolysis of peanut shells into three distinct peaks representing material components: P-Lig, P-Cell, and P-Hem. The Gaussian equation is defined as Equation (1).

$$y = y_0 + \frac{B}{w\sqrt{\frac{\pi}{4\ ln\ 2}}} exp\left[\frac{-4\ ln(2)*(T - T_p)^2}{w^2}\right] \quad (1)$$

where y_0, B, and T_p represent the base, peak area, and peak temperature, respectively. Moreover, w denotes the shape parameter. Meanwhile, T denotes the fitted peak temperature.

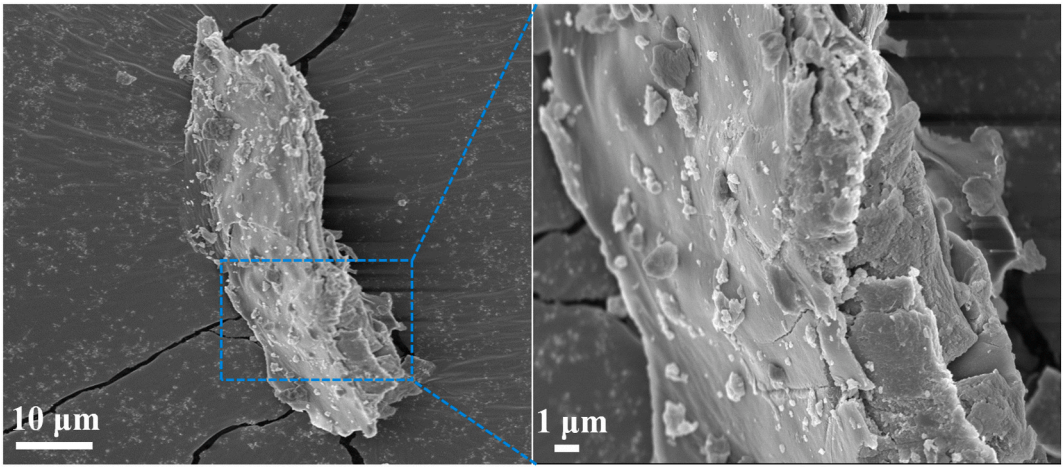

Fig. 3. Micromorphology of peanut shell.

Due to the intricacy of pyrolysis, model errors are unavoidable. To assess the validity of the model, the fit quality between calculated and experimental values was evaluated through mathematical comparison using the coefficient of determination (R^2) as described in Equation (2) [45].

$$R^2 = 1 - \frac{\sum_{i=1}^{N} \left(x_{exp} - x_{dec}\right)^2}{\sum_{i=1}^{N} \left(x_{exp} - x_{ave}\right)^2} \tag{2}$$

where x_{exp}, x_{ave}, and x_{dec} represent the measured values, the average of experimental data, and the values obtained from deconvolution, respectively. The subscript i is the experimental data point. Meanwhile, N represents the number of experimental data points utilized for the deconvolution. It should be indicated that x can represent either the conversion rate ($d\alpha/dt$) or conversion degree (α).

2.4. Experimental procedure

Thermogravimetric testing was performed utilizing a thermogravimetric analyzer (TGA5500, Waters, USA). Each sample, weighing approximately 10 ± 0.5 mg, was put inside analumina crucible and underwent heating at three different rates: 10 K/min, 20 K/min, and 30 K/min, starting from room temperature and reaching 1173 K, all at atmospheric pressure. The heating rate is low enough to ensure efficient uniform decomposition while minimizing mass and heat transfer effects. Throughout the entire pyrolysis process, a 120 mL/min flow of N_2 with a purity of 99.999 % was used. To minimize vibration errors, each heating rate experiment was performed in triplicate.

2.5. Kinetic method

The pyrolysis of biomass is an intricate process. To this end, it is assumed that the pyrolysis of peanut shells can be explained by three parallel processes, where P-Hem, P-Cell, and P-Lig decompose independently, generating char and volatiles according to the following process: A (biomass)→B (char) + C (volatiles). This model has demonstrated promising results in various studies focusing on lignocellulosic biomass pyrolysis. For single-step pyrolysis reactions, the conversion can be explained as follows [46]:

$$\frac{d\alpha}{dt} = k(T) f(\alpha) \tag{3}$$

where $f(\alpha)$ denotes the differential expression of the reaction model, $k(T)$ denotes the pyrolysis rate constant, t denotes the pyrolysis time. The parameter α can be obtained by thermogravimetric analysis data, using Equation (4).

$$\alpha = \frac{m_0 - m_t}{m_0 - m_\infty} \tag{4}$$

where m_0, m_t, and m_∞ denote the initial, instant, and residual mass of biomass during the pyrolysis process, respectively. Based on the Arrhenius law, $k(T)$ can be presented as follows:

$$k(T) = A \exp\left(-\frac{E_\alpha}{RT}\right) \tag{5}$$

where A is the pre-exponential factor, E_α is the apparent activation energy and R represents the universal gas constant. Combining Equations (3) and (5) at a given constant ($\beta = dT/dt$), yields Equation (6).

$$\frac{d\alpha}{dT} = \frac{A}{\beta}\exp\left(-\frac{E_\alpha}{RT}\right) f(\alpha) \tag{6}$$

The integral form of $f(\alpha)$ is described as Equation (7).

$$\int_0^\alpha \frac{d\alpha}{f(\alpha)} = g(\alpha) = \frac{A}{\beta}\int_{T_0}^{T} e^{-\frac{E_\alpha}{RT}} dT \tag{7}$$

2.5.1. Model-free methods

In model-free methods, the reaction kinetics does not directly relate to β. Studies show that among mathematical approaches, the KAS and FWO methods demonstrate good adaptability, validity, and accuracy for acquiring kinetic parameters. Accordingly, these methods were employed in the present study. The FWO method utilizes Doyle's approximation for temperature integration in the form of Equation (8) [47–49].

$$\ln\beta = \ln\frac{AE_\alpha}{g(\alpha)R} - 5.331 - 1.052\frac{E_\alpha}{RT} \tag{8}$$

Accordingly, $E\alpha$ can be calculated from the slope $-1.052E\alpha/R$ of the regression lines for FWO method. The KAS method can be represented in the form below [50]:

$$\ln\frac{\beta}{T^2} = \ln\frac{AR}{E_\alpha g(\alpha)} - \frac{E_\alpha}{RT} \tag{9}$$

Equation (9) indicates that $E\alpha$ can be calculated using the slope $-E\alpha/R$ of the regression lines for KAS method.

2.5.2. Vyazovkin method

Vyazovkin has developed an nonlinear method to obtain the $E\alpha$ based on numerical integral [51,52]. The advantage of this advanced isoconversional method is that it is not limited to linear temperature schedules, and it takes the possible fluctuations of the activation energyinto account. According to this method, the activation energy can be assessed by finding the value of $E\alpha$ that minimizes Equation (10) [53].

$$\varnothing(E_\alpha) = \sum_{i=1}^{n}\sum_{j\neq 1}^{n}\frac{I(E_\alpha, T_i)\beta_j}{I(E_\alpha, T_j)\beta_i} \tag{10}$$

where the indexes i and j denote the set of experiments conducted at various heating rates, and n is the total number of experiments carried out. The temperature integral is defined as:

$$I(E_\alpha, T) = \int_0^T \exp(-E_\alpha / RT)dT \tag{11}$$

The following fourth-degree approximation as described in Equations (12) and (13) proposed by Senum and Yang [54] was used to evaluate equation (11).

$$I(E_\alpha, T) = \frac{E_\alpha}{R}h(x) \tag{12}$$

$$h(x) = \frac{x^4 + 18x^3 + 86x^2 + 96x}{x^4 + 20x^3 + 120x^2 + 240x + 120} \tag{13}$$

2.5.3. Model-fitting methods

The model-fitting methods seek the most suitable reaction mechanism function. In this investigation, the CR method was employed to study the reaction mechanism. This can be mathematically expressed as Equation (14) [55].

$$\ln\frac{g(\alpha)}{T^2} = \ln\frac{AR}{\beta E_\alpha} - \frac{E_\alpha}{RT} \tag{14}$$

The $E\alpha$ value can be obtained by the slope of the regression lines of $\ln g(\alpha)/T^2$ versus $1/T$. If the mean calculated value obtained from the model-fitting and model-free methods are consistent, the corresponding reaction model is suitable for simulating single-step pyrolysis reactions. The chemical reaction order, diffusion, phase boundary reaction, random nucleation, diffusional, and exponential nucleation are the main categories into which the mechanisms of reactions for biomass pyrolysis can be divided. This article selected 22 pyrolysis reaction models as listed in Table 3 [56–59].

2.6. Thermodynamic method

Based on the activation energycomputed using the FWO and KAS methods, the pre-exponential factor A and thermodynamic parameters, like enthalpy (ΔH), Gibbs free energy (ΔG), and entropy (ΔS), can be determined by Equations (15)–(18) [60].

$$A = \frac{\beta E_\alpha \exp\left(\frac{E_\alpha}{RT_m}\right)}{RT_m^2} \tag{15}$$

$$\Delta H = E_\alpha - RT \tag{16}$$

$$\Delta G = E_\alpha + RT_m \ln\left(\frac{K_B T_m}{hA}\right) \tag{17}$$

$$\Delta S = \frac{\Delta H - \Delta G}{T_m} \tag{18}$$

where $k_B = 1.381 \times 10^{-23}$ J/K represents the Boltzmann constant and $h = 6.626 \times 10^{-34}$ J/s is Planck's constant. The values of A at each conversion degree can be assessed from Kissinger's method [61].

3. Results and discussions

3.1. Thermogravimetric analysis

Fig. 4 illustrates the TG and DTG plots of the peanut shell pyrolysis process under an N_2 atmosphere at various ramp rates. It is found that as the heating rate increases from 10 K/min–30 K/min, the rate of massloss and peak temperature shifts to higher

Table 3
Common mechanism functions of solid-state thermal reaction.

Mechanism	symbol	$f(\alpha)$	$g(\alpha)$
Diffusion	D	Differential form	Integral form
1D diffusion	D_1	$1/2\alpha$	α^2
2D diffusion	D_2	$[-\ln(1-\alpha)]^{-1}$	$\alpha + (1-\alpha)\ln(1-\alpha)$
3D diffusion (Jander)	D_3	$\left[(3/2)(1-\alpha)^{2/3}\right]/\left[1-(1-\alpha)^{1/3}\right]$	$\left[1-(1-\alpha)^{1/3}\right]^2$
3D diffusion (Ginstling-Brounshtein)	D_4	$(3/2)\left[(1-\alpha)^{-1/3}-1\right]^{-1}$	$(1-2\alpha/3)-(1-\alpha)^{2/3}$
3D diffusion (Zhuravleve-Lesokine)	D_5	$\left[(3/2)(1-\alpha)^{4/3}\right]/\left[(1-\alpha)^{-1/3}-1\right]$	$\left[(1-\alpha)^{-1/3}-1\right]^2$
3D diffusion	D_6	$\left[(3/2)(1+\alpha)^{2/3}\right]/\left[(1+\alpha)^{1/3}-1\right]$	$\left[(1+\alpha)^{1/3}-1\right]^2$
Chemical reaction order	F	Differential form	Integral form
First-order	F_1	$1-\alpha$	$-\ln(1-\alpha)$
Second-order	F_2	$(1-\alpha)^2$	$(1-\alpha)^{-1}-1$
Third-order	F_3	$1/2(1-\alpha)^3$	$(1-\alpha)^{-2}-1$
Fourth-order	F_4	$1/3(1-\alpha)^4$	$(1-\alpha)^{-3}-1$
Random nucleation and subsequent growth	A	Differential form	Integral form
Avrami-Erofeyev	A_2	$2(1-\alpha)[-\ln(1-\alpha)]^{1/2}$	$[-\ln(1-\alpha)]^{1/2}$
Avrami-Erofeyev	A_3	$3(1-\alpha)[-\ln(1-\alpha)]^{2/3}$	$[-\ln(1-\alpha)]^{1/3}$
Avrami-Erofeyev	A_4	$4(1-\alpha)[-\ln(1-\alpha)]^{3/4}$	$[-\ln(1-\alpha)]^{1/4}$
Avrami-Erofeyev	$A_{1/2}$	$1/2(1-\alpha)[-\ln(1-\alpha)]^{-1}$	$[-\ln(1-\alpha)]^2$
Avrami-Erofeyev	$A_{1/3}$	$1/3(1-\alpha)[-\ln(1-\alpha)]^{-2}$	$[-\ln(1-\alpha)]^3$
Avrami-Erofeyev	$A_{1/4}$	$1/4(1-\alpha)[-\ln(1-\alpha)]^{-3}$	$[-\ln(1-\alpha)]^4$
Phase boundary reaction	R	Differential form	Integral form
Contracting disk	R_1	1	α
Contracting cylinder	R_2	$2(1-\alpha)^{1/2}$	$1-(1-\alpha)^{1/2}$
Contracting sphere	R_3	$3(1-\alpha)^{2/3}$	$1-(1-\alpha)^{1/3}$
Acceleratory rate equations	P	Differential form	Integral form
Nucleation	$P_{1/2}$	$2\alpha^{1/2}$	$\alpha^{1/2}$
Nucleation	$P_{1/3}$	$3\alpha^{2/3}$	$\alpha^{1/3}$
Nucleation	$P_{1/4}$	$4\alpha^{3/4}$	$\alpha^{1/4}$

temperatures. The pyrolysis process consists of three stages based on the DTG profiles. Stage I (<428 K) is accompanied by negligible mass loss, with an average mass loss of 8.69 %, 8.71 %, and 8.72 % at heating rates of 10 K/min, 20 K/min, and 30 K/min, respectively. This stage primarily corresponds to the evaporation of moisture and small molecules of volatile substances. Stage II (428 K–973 K) was the major pyrolysis stage of the peanut shell, attributed to devolatilization. The sample lost the most weight in this stage, the maximum pyrolysis rates exposed to heating rates of 10 K/min, 20 K/min, and 30 K/min were 4.95 %/min, 9.67 %/min, and 13.82 %/min, respectively. In this zone, one sharper peak and one long tail can be observed on the DTG curve, corresponding to the pyrolysis of the main biomass components. These overlaps suggest a parallel reaction kinetic model, where hemicellulose, cellulose, and lignin undergo independent decomposition throughout the pyrolysis process. Stage III primarily occurred after 973 K and involved the charring process of the carbonaceous degradation of residues. Finally, the residual masses were 21.43 %, 20.74 %, and 20.89 %, respectively. In this stage, as the temperature increased, the TG curve was affected slightly, while the DTG curve approached zero. The results demonstrate that stage II is the main pyrolysis stage, thus kinetic analysis was performed only in this stage. This phenomenon is primarily due to the concurrent degradation of biomass components, challenging the distinction of the degradation behaviors of each component. Therefore, deconvolving the overlapped peaks into corresponding individual P-Com is of significant importance to elucidate their contributions to degradation by exploring kinetic parameters.

3.2. DTG/TGA curve deconvolution

The thermochemical process of peanut shell pyrolysis is indeed quite complex, often associated with its main components. In this study, the Gaussian function was utilized to deconvolute the reaction rate $d\alpha/dT$ and conversion α using integral deconvolution in stage II of the TG/DTG data for various heating rates. The results are presented in Figs. 5 and 6.

Three deconvolution profiles were observed with temperature ranges of 428 K–660 K, 560 K–860 K, and 600 K–973 K at a heating rate of 10 K/min, with maximum mass loss peak temperatures of 575.72 K, 726.14 K, and 865.97 K, respectively. Studies [62,63]

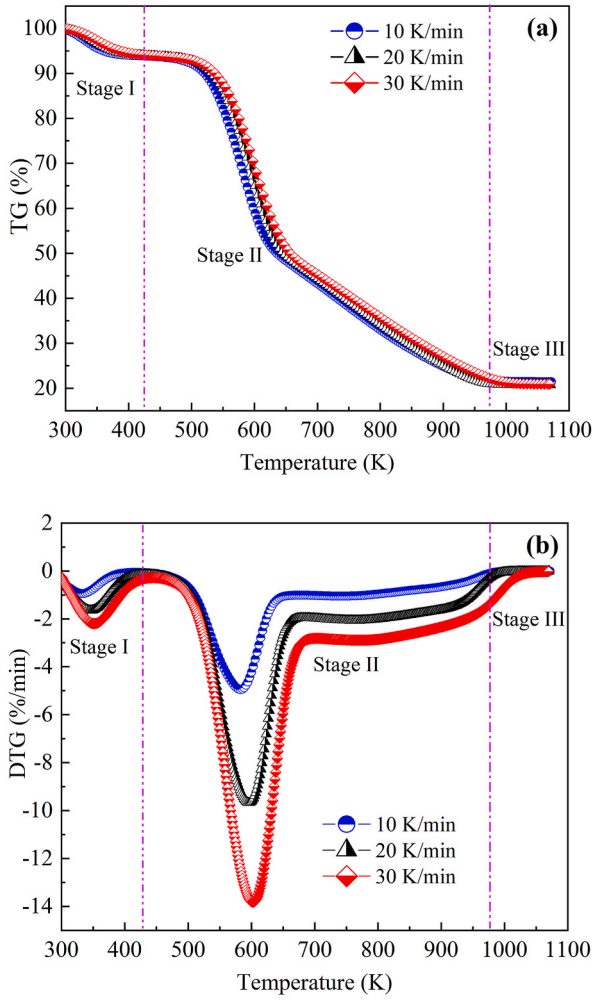

Fig. 4. The plots of the peanut shell pyrolysis process (a) TG; (b) DTG.

demonstrate that the pyrolysis temperature ranges of hemicellulose, cellulose, and lignin are 473 K–633 K, 573 K–763 K, and 473 K–1063 K, respectively. The pyrolysis intervals of each P-Com exhibited significant overlap with the literature values, suggesting that the three deconvolution profiles were likely attributed to the thermal decomposition of P-Hem, P-Cell, and P-Lig. The corresponding parameters (y_0, B, Tp, and w) for Guassian function were listed in Table 4.

It is inferred that the Gaussian function successfully deconvoluted the peanut shell, with R^2 values consistently exceeding 0.994 at various heating rates. Additionally, it was feasible to further derive the reaction rate dα/dT and conversion α for each P-Com curve

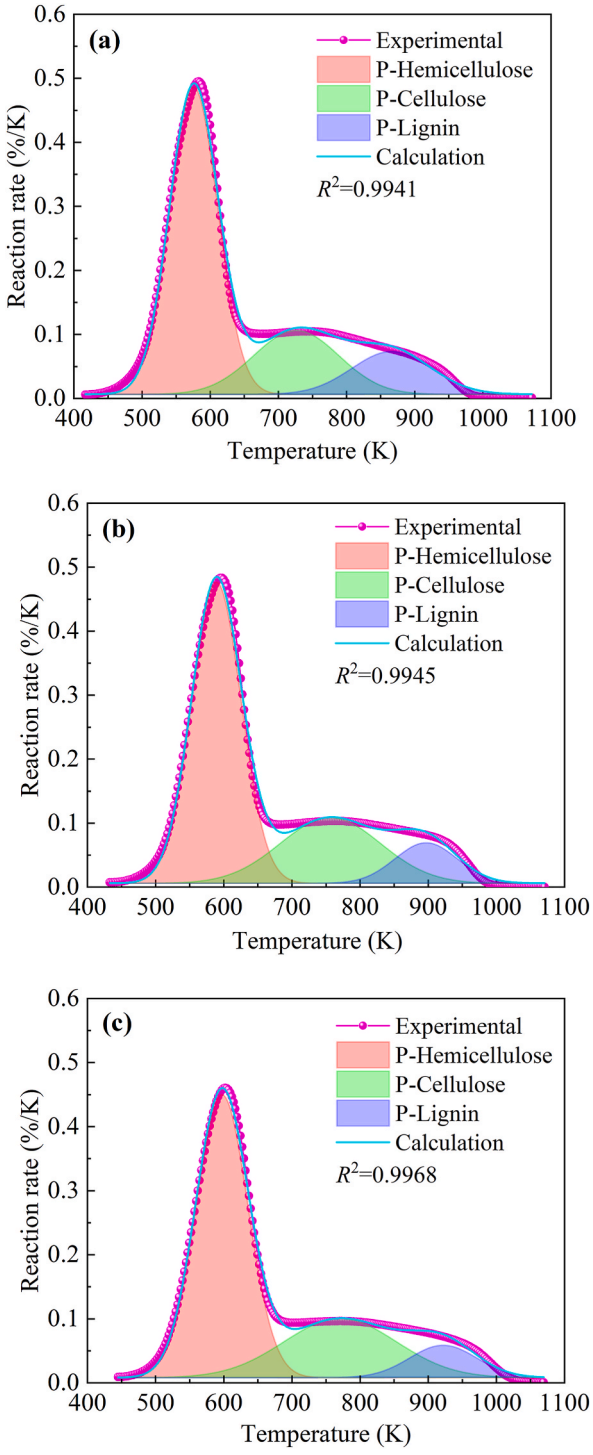

Fig. 5. The distribution of the reaction rate dα/dT deconvolved by Gaussian function (a) 10 K/min; (b) 20 K/min; (c) 30 K/min.

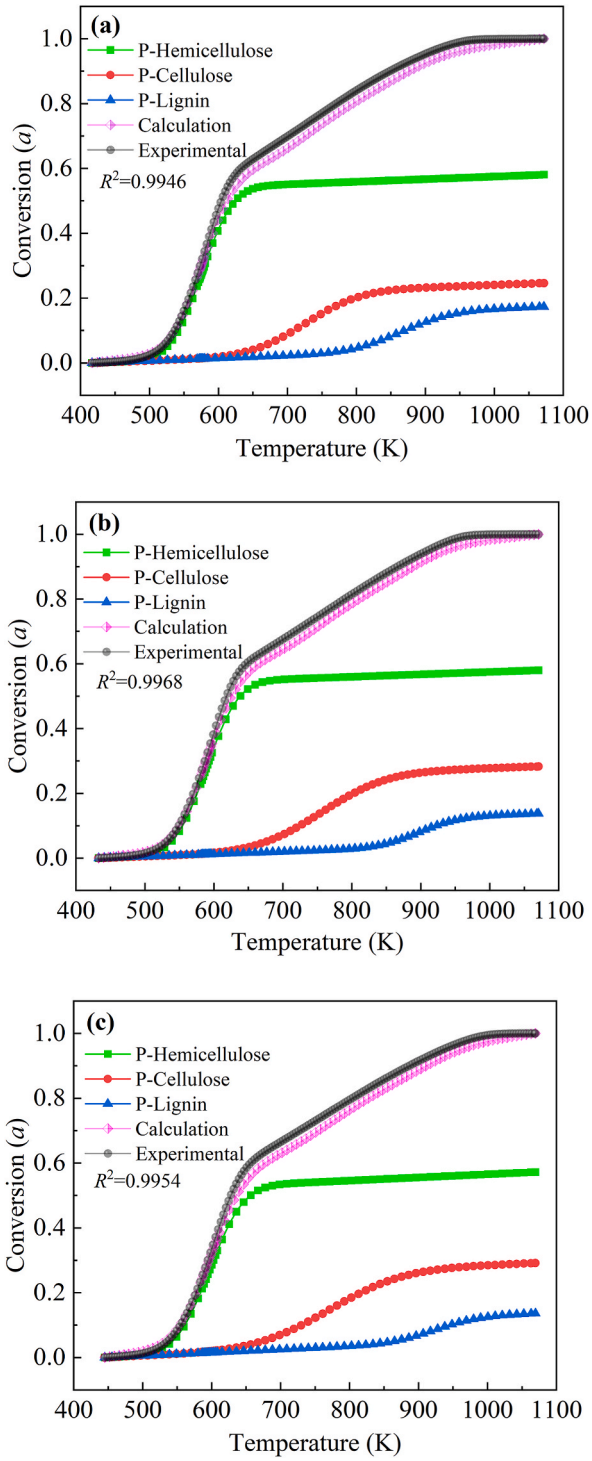

Fig. 6. The distribution of the conversion α deconvolved by Gaussian function (a) 10 K/min; (b) 20 K/min; (c) 30 K/min.

with temperature based on the deconvolution results. These parameters are essential for subsequent kinetic analysis.

3.3. Kinetics analysis of pseudo components

The KAS and FWO methods were employed to fit the experimental thermogravimetric data of the three P-Coms to determine the

Table 4
The corresponding parameters for Guassian function.

Heating Rate (K/min)	Pseudo Components	y_0	B	Tp	w
10	P-Hem	0.00647	42.74	575.72	71.03
	P-Cell	0.00647	18.69	726.14	125.26
	P-Lig	0.00647	7.81	865.97	116.66
20	P-Hem	0.00605	43.08	589.13	72.99
	P-Cell	0.00605	19.20	756.46	147.68
	P-Lig	0.00605	7.27	897.03	91.60
30	P-Hem	0.00818	42.52	597.14	76.81
	P-Cell	0.00818	19.17	770.71	165.41
	P-Lig	0.00818	6.75	921.85	98.57

apparent activation energy at various α values. The fitting results are presented in Figs. 7 and 8. For both methods, the conversion degree in the range of 0.10–0.85 with a 0.05 increment was chosen, as correlation values outside of this range were found to be low.

The calculated activation energy values are summarized in Tables 5–7, indicating that the values of determination coefficients R^2 obtained by the KAS and FWO methods ranged from 0.981 to 1.0 and 0.978 to 1.0, respectively, and all the mean squared error values (MSE) were less than 0.014. This observation demonstrates excellent linear fitting of the results. Furthermore, the results are consistent, with the KAS method yielding slightly lower values. For the KAS method, the activation energy $E\alpha$ values for P-Hem pyrolysis ranged from 126.25 kJ/mol to 139.39 kJ/mol (Average 133.89 kJ/mol), for P-Cell ranged from 92.58 kJ/mol to 161.37 kJ/mol (Average 115.44 kJ/mol), and for P-Lig ranged from 145.66 kJ/mol to 227.90 kJ/mol (Average 174.31 kJ/mol). On the other hand, for the FWO technique, the $E\alpha$ values for P-Hem pyrolysis ranged from 129.76 kJ/mol to 140.99 kJ/mol (Average 136.53 kJ/mol), for P-Cell ranged from 100.99 kJ/mol to 163.74 kJ/mol (Average 120.33 kJ/mol), and for P-Lig ranged from 152.13 kJ/mol to 226.30 kJ/mol (Average 177.79 kJ/mol). The activation energy values obtained by Vyazoykin method are listed in Tables 5–7 as well. By minimizing Equation (10), the $E\alpha$ values for P-Hem pyrolysis ranged from 129.13 kJ/mol to 137.12 kJ/mol (Average 134.29 kJ/mol), for P-Cell ranged from 96.67 kJ/mol to 158.92 kJ/mol (Average 116.61 kJ/mol), and for P-Lig ranged from 147.12 kJ/mol to 226.26 kJ/mol (Average 174.96 kJ/mol). The apparent activation energy $E\alpha$ provides the minimum energy barrier that must be overcome prior to the initiation of the reaction and the formation of products [64]. The average values of $E\alpha$ for the three P-Coms calculated using the KAS, FWO, and Vyazoykin methods exhibited a similar trend: P-Lig > P-Hem > P-Cell. These results suggest that cellulose is more readily decomposed than hemicellulose, while the decomposition of lignin is the most challenging. This observation can be elucidated by the fact that lignin is composed of aromatic compounds with long carbon chains, requiring more energy to break down compared to cellulose and hemicellulose.

3.4. Reaction mechanism of P-Com

The investigation of the reaction mechanismin the primary pyrolysis stageof each P-Com at different heating rates was conducted using the CR method, while the average apparent activation energy was calculated using the KAS, FWO, and Vyazoykin methods, and the mechanisms for the pyrolysis of solid biomass are provided in Table 3. If the average Ea calculated using the CR method closely matches that acquired by the KAS, FWO, and Vyazoykin methods for each P-Com, an appropriate reaction mechanism can be identified, the detailed results are shown in Tables 8–10. It was observed that the average activation energy (138.61 kJ/mol) for P-Hem calculated by the random nucleation mechanism $A_{1/2}$ at various heating rates based on the CR method approximates the values (136.53 kJ/mol, 133.89 kJ/mol, and 134.29 kJ/mol) calculated using the FWO, KAS, and Vyazoykin methods, with deviations of 1.5 %, 3.5 %, and 3.1 %, respectively. Accordingly, it is inferred that the $A_{1/2}$ random nucleation model better describes the pyrolysis process for P-Hem. Similarly, it can be inferred that the optimal model for the pyrolysis of P-Cell follows the random nucleation model $A_{1/2}$ (As shown in Table 9), and for P-Lig follows the diffusional reaction mechanism D_5 (As shown in Table 10). The R^2 dependence of all P-Com in the best-fit reaction mechanisms is greater than 0.985, and the maximum deviation is less than 3.5 %, indicating that the pyrolysis models for P-Lig, P-Cell, and P-Hem were accurately predicted by the CR model.

3.5. The kinetics compensation effect

Considering that conversion degree is a factor causing the changes of the Arrhenius parameters, Equation $\ln A = aE_\alpha + b$ can be used to predict the kinetic compensation effect (KCE) [61], where a and b are the kinetic compensation parameters. In order to observe the KCE in the peanut shells pyrolysis process, the correlation between the activation energy $E\alpha$ and the pre-exponential factor $\ln A$ for each P-Com is plotted in Fig. 9. The intense linear relationship between the $E\alpha$ and the $\ln A$ confirms the KCE, allowing the conversion degree at different heating rates to be modeled. The kinetic compensation parameters for each P-Com are shown in Table 11.

3.6. Thermodynamic analysis

Since the thermodynamic parameters were basically not affected by the heating rate, the values of thermodynamic parameters such as change of enthalpy (ΔH), change of Gibb's free energy (ΔG), and change of entropy (ΔS) at the heating rate of 10 K/min using the

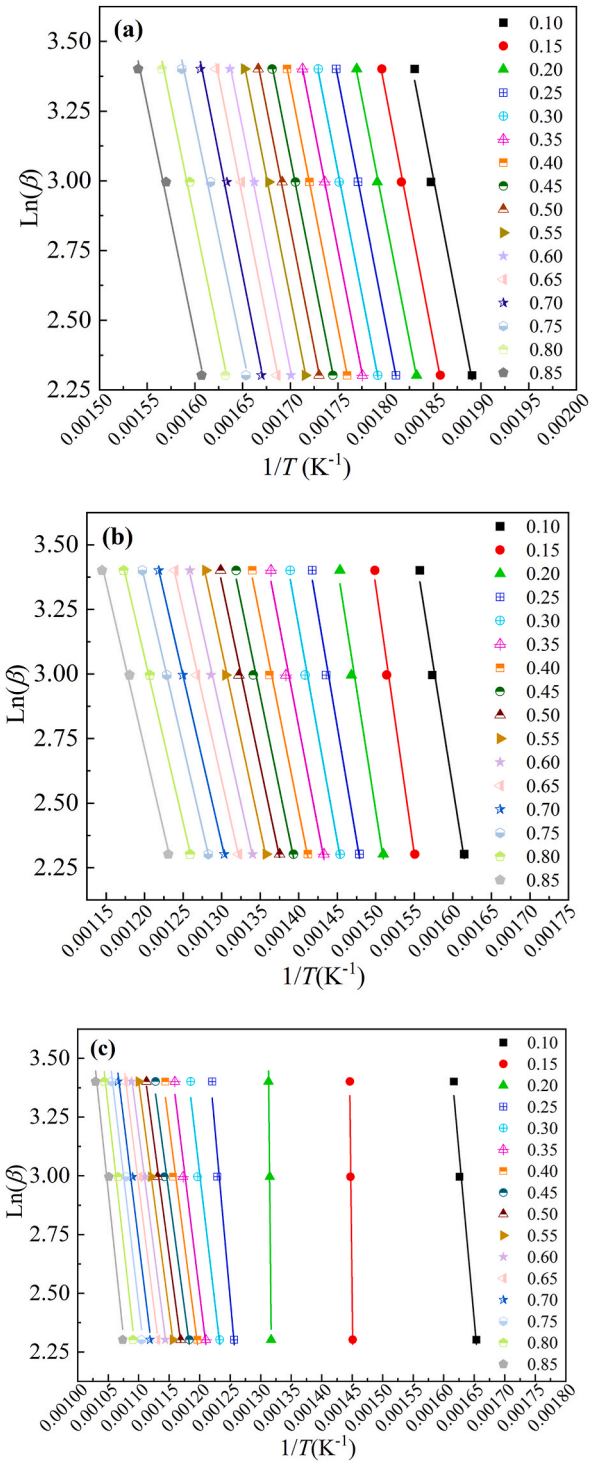

Fig. 7. The fitting results of the FWO methods (a) pseudo-hemicellulose; (b) pseudo-cellulose; (c) pseudo-lignin.

FWO, KAS, and Vyazoykin methods, including the KCE, are shown in Tables 12–14. All calculated ΔH values using the three model-free methods are positive, indicating that the pyrolytic reactions of peanut shells are endothermic. The mean differences between the $E\alpha$ and ΔH values for P-Hem, P-Cell, and P-Lig are lower than 4.8 kJ/mol, 6.0 kJ/mol, and 6.9 kJ/mol, respectively, indicating that the product generation is favorable [65]. The higher the ΔG value, the lower the pyrolysis reaction favorability. It can seen that, the change in ΔG for P-Hem, P-Cell, and P-Lig using the three model-free methods are stable within the range of 166.96 kJ/mol to 167.48 kJ/mol,

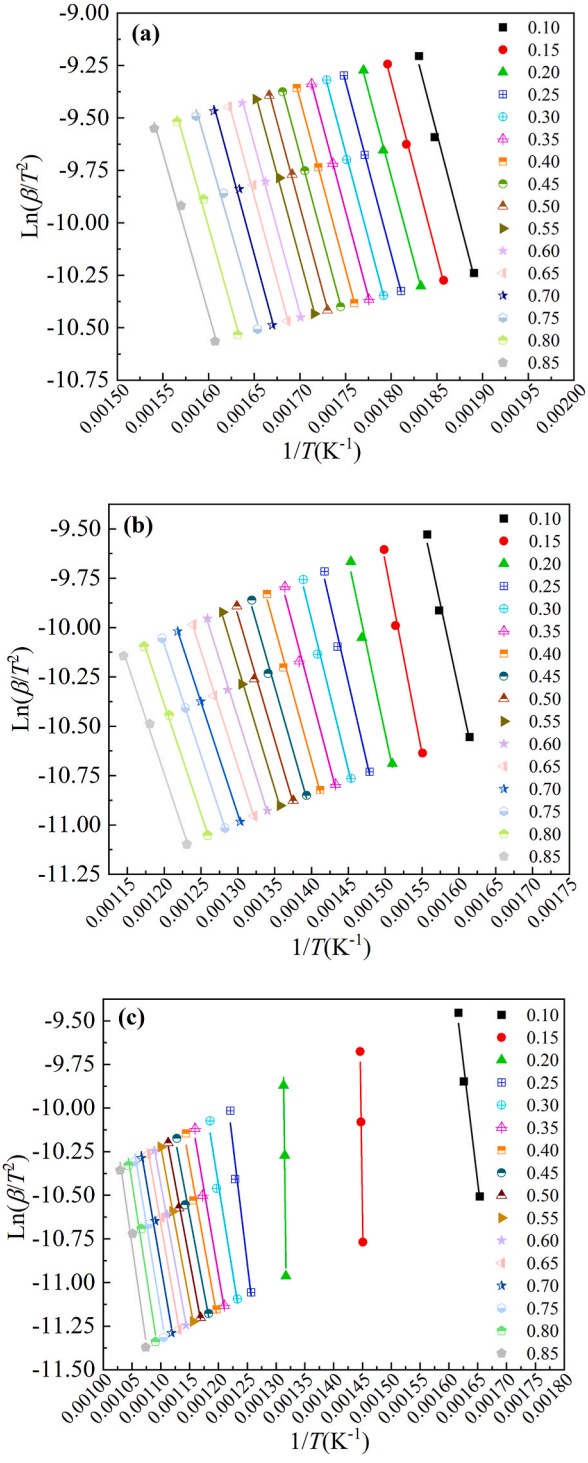

Fig. 8. The fitting results of the KAS methods (a) pseudo-hemicellulose; (b) pseudo-cellulose; (c) pseudo-lignin.

213.88 kJ/mol to 217.05 kJ/mol, and 256.49 kJ/mol to 259.71 kJ/mol, respectively, indicating that more energy is required for lignin pyrolysis. The degree of reaction disorder was defined as ΔS. All calculated ΔS values by the three model-free methods are negative, indicating that the degree of disorder in the activated complex is lower than those in the reactants. The higher ΔG values and negative ΔS values for P-Lig suggested that the thermal degradation of lignin is slow [66]. The thermodynamic analysis revealed that the decomposition of peanut shell is endothermic and non-spontaneous. Additionally, the values of ΔG vary within ± 2 kJ/mol for each

Table 5
The calculated apparent activation energy using FWO, KAS, and Vyazoykin methods for P-Hem.

α	FWO			KAS			Vyazoykin
	$E\alpha$ (kJ/mol)	R^2	MSN	$E\alpha$ (kJ/mol)	R^2	MSN	$E\alpha$ (kJ/mol)
0.10	140.99	0.991	0.0053	139.39	0.990	0.0053	137.12
0.15	140.89	0.998	0.0009	139.12	0.998	0.0009	136.92
0.20	137.39	0.999	0.0005	135.31	0.999	0.0005	135.36
0.25	138.61	1.0	0	136.48	1.0	0	136.46
0.30	138.26	0.999	0.0003	136.01	0.999	0.0001	135.44
0.35	138.30	1.0	0	135.96	1.0	0	134.79
0.40	137.88	1.0	0	135.44	1.0	0	135.26
0.45	136.94	0.999	0.0001	134.35	0.999	0.0001	134.23
0.50	136.85	0.999	0.0005	134.18	0.999	0.0001	133.54
0.55	136.69	0.998	0.0007	133.92	0.998	0.0005	133.32
0.60	136.39	0.998	0.0007	133.52	0.998	0.0007	134.34
0.65	136.29	0.997	0.0018	133.33	0.996	0.0018	134.23
0.70	136.64	0.994	0.0032	133.59	0.993	0.0033	136.41
0.75	129.76	0.991	0.0052	126.25	0.990	0.0053	129.13
0.80	131.63	0.994	0.0037	128.07	0.992	0.0038	131.40
0.85	131.07	0.993	0.0039	127.32	0.992	0.0040	130.70
Average	136.53			133.89			134.29

Table 6
The calculated apparent activation energy using FWO, KAS, and Vyazoykin methods for P-Cell.

α	FWO			KAS			Vyazoykin
	$E\alpha$ (kJ/mol)	R^2	MSN	$E\alpha$ (kJ/mol)	R^2	MSN	$E\alpha$ (kJ/mol)
0.10	147.26	0.990	0.0059	144.44	0.989	0.0059	142.47
0.15	163.74	0.993	0.0042	161.37	0.992	0.0042	158.92
0.20	149.19	0.987	0.0081	145.73	0.985	0.0080	145.81
0.25	138.75	0.992	0.0046	134.49	0.991	0.0046	134.87
0.30	131.24	0.993	0.0039	126.38	0.992	0.0038	127.18
0.35	123.44	0.991	0.0056	117.98	0.989	0.0055	118.74
0.40	118.48	0.995	0.0029	112.57	0.994	0.0029	113.99
0.45	114.66	0.994	0.0036	108.37	0.992	0.0036	109.94
0.50	111.90	0.995	0.0027	105.29	0.994	0.0027	106.34
0.55	109.90	0.998	0.0010	103.01	0.998	0.0009	104.18
0.60	106.02	0.998	0.0009	98.75	0.998	0.0009	101.17
0.65	104.35	0.999	0.0006	96.81	0.998	0.0006	99.38
0.70	102.28	1.0	0	112.91	1.0	0	111.21
0.75	101.68	1.0	0	93.57	1.0	0	97.86
0.80	100.99	0.999	0.0005	92.58	0.998	0.0006	96.67
0.85	101.46	0.997	0.0017	92.74	0.996	0.0018	96.94
Average	120.33			115.44			116.61

P-Com, indicating that peanut shell can be converted into value-added sources of energy steadily through pyrolysis process [67].

3.7. Energy balance and future applications

The data from the experiments made at the intermediate temperature of 773 K were used to perform an energy balance. The higher heating value of peanut shell was 18.46 MJ/kg, which was estimated by the empirical correlations [68]. The energetic value of the gas products [69] was assessed to be 1.42 MJ/kg for peanut shell pyrolysis. The total energy from the pyrolysis products was evaluated to be 17.18 MJ/kg. Therefore, 1.28 MJ/kg was required to decompose the pecan shells, which is within the range reported for various biomasses [70]. Thus, the energy content of the pyrolysis gases is enough to energetically sustain the pyrolysis process at 773 K.

Therefore, pyrolysis is a promising valorization pathway for the applications of peanut shells. They canbe transform into rich gas products, biochar, and high-quality bio-oil by pyrolysis, where bio-oil can be used in an internal combustion engine, biochar can be used to produced biochar briquette with high carbon content, high calorific value and less toxic gas emitted during combustion or can be alternatively used as soil amendment, and gas products can be used as a clean gas energy source. In addition, peanut shells can be used as a biomass boiler to generate electricity through combustion.

4. Conclusions

In this study, the peak-differentiating analysis with the Gaussian function was employed to separate the pyrolysis of peanut shells

Table 7
The calculated apparent activation energy using FWO, KAS, and Vyazoykin methods for P-Lig.

α	FWO			KAS			Vyazoykin
	Eα (kJ/mol)	R^2	MSN	*Eα* (kJ/mol)	R^2	MSN	*Eα* (kJ/mol)
0.10	226.30	0.985	0.0103	227.90	0.982	0.0103	222.82
0.15	179.41	0.985	0.0103	187.60	0.983	0.0103	181.17
0.20	208.38	0.980	0.0124	217.95	0.981	0.0124	213.17
0.25	229.01	0.978	0.0135	227.51	0.978	0.0135	226.26
0.30	174.29	0.978	0.0129	169.61	0.978	0.0129	170.08
0.35	165.92	0.987	0.0089	160.53	0.984	0.0088	160.90
0.40	158.15	0.981	0.0128	152.18	0.978	0.0127	153.44
0.45	152.13	0.984	0.0084	145.66	0.984	0.0083	147.12
0.50	153.61	0.998	0.0013	147.04	0.997	0.0013	147.64
0.55	154.99	1.0	0	148.33	1.0	0	148.94
0.60	158.34	0.998	0.0009	151.68	0.998	0.0010	153.90
0.65	163.78	0.991	0.0056	157.23	0.990	0.0057	159.51
0.70	166.23	0.989	0.0069	159.65	0.988	0.0069	164.53
0.75	174.34	0.982	0.0112	168.01	0.980	0.0113	172.94
0.80	184.03	0.984	0.0099	178.02	0.983	0.0010	182.44
0.85	195.77	0.981	0.0118	190.13	0.980	0.0119	194.58
Average	177.79			174.31			174.96

Table 8
The apparent activation energy acquired by the CR method for P-Hem.

Mechanism	10 K/min		20 K/min		30 K/min		Average (kJ/mol)
	Eα (kJ/mol)	R^2	*Eα* (kJ/mol)	R^2	*Eα* (kJ/mol)	R^2	
D_1	93.28	0.936	97.32	0.941	91.47	0.941	94.03
D_2	108.23	0.958	112.67	0.962	106.05	0.961	108.98
D_3	123.44	0.978	128.48	0.980	120.24	0.979	124.05
D_4	114.48	0.966	119.07	0.979	112.11	0.968	115.22
D_5	170.39	0.996	176.16	0.997	166.27	0.996	170.94
D_6	81.00	0.922	84.60	0.928	79.38	0.929	81.66
F_1	64.02	0.982	71.50	0.989	67.08	0.988	67.53
F_2	106.41	0.999	109.81	0.999	103.40	0.999	106.54
F_3	160.17	0.992	157.40	0.990	148.51	0.993	155.36
F_4	221.22	0.983	211.68	0.979	199.96	0.983	210.95
A_2	29.61	0.983	30.77	0.984	28.49	0.982	29.63
A_3	16.50	0.974	17.22	0.977	15.64	0.973	16.45
A_4	9.95	0.959	10.43	0.964	9.20	0.955	9.86
$A_{1/2}$	137.87	0.990	138.26	0.991	139.71	0.992	138.61
$A_{1/3}$	226.28	0.990	234.36	0.991	221.41	0.990	227.35
$A_{1/4}$	304.95	0.990	315.79	0.991	298.57	0.990	306.44
G_1	45.44	0.877	43.70	0.927	40.69	0.926	43.27
G_2	56.67	0.937	56.31	0.967	52.66	0.965	55.21
G_3	60.97	0.952	61.08	0.976	57.19	0.974	59.75
P_1	21.68	0.883	16.89	0.881	15.30	0.873	17.96
P_2	11.27	0.816	7.95	0.781	6.84	0.749	8.69
P_3	6.08	0.690	3.48	0.542	2.61	0.427	4.06

into three independent one-step reactions, corresponding primarily to hemicelluloses, cellulose, and lignin decomposition. After deconvolution, the pyrolysis kinetics, pyrolysis mechanisms, and thermodynamic parameters of each P-Com were obtained and validated. The mean apparent activation energy values generally followed an order of P-Lig > P-Hem > P-Cell, estimated at 174.31 kJ/mol, 133.89 kJ/mol, and 115.44 kJ/mol by KAS, 177.79 kJ/mol, 136.53 kJ/mol, and 120.33 kJ/mol by FWO, and 174.96 kJ/mol, 134.29 kJ/mol, and 116.61 kJ/mol by Vyazoykin, respectively. The CR model-fitting method was employed to ascertain the pyrolysis mechanism, revealing that the mechanism function $A_{1/2}$is the most suitable reaction model for P-Hem and P-Cell pyrolysis, while for P-Lig pyrolysis, the best-fit model was the diffusional reaction mechanism D_5. Thermodynamic parameters indicated that the pyrolysis of peanut shell was endothermic and non-spontaneous. It can be steadily converted into value-added energy through pyrolysis with the values of ΔG vary within ± 2 kJ/mol for each P-Com. This study demonstrated that the Gaussian deconvolution function can significantly enhance the understanding of the peanut shell pyrolysis process. Such insights are crucial for comprehensively understanding the thermal conversion process of peanut shell and for effectively utilizing agricultural waste resources. However, in this study, the discussion mainly foucus on the pyrolysis mechanism of peanut shell powder with particle size of 80–106 μm. The results are hardly sufficient for scaling up the system. In order to better guide industrial application for the pyrolysis of peanut shells, a subsequent paper will focus on a detailed analysis of the effect of pyrolysis temperature on physicochemical properties of pyrolysis products with different particle sizes using a laboratory scale fixed-bed reactor.

Table 9
The apparent activation energy acquired by the CR method for P-Cell.

Mechanism	10 K/min		20 K/min		30 K/min		Average (kJ/mol)
	$E\alpha$ (kJ/mol)	R^2	$E\alpha$ (kJ/mol)	R^2	$E\alpha$ (kJ/mol)	R^2	
D_1	74.59	0.965	73.11	0.971	64.60	0.973	70.77
D_2	86.46	0.978	84.63	0.983	74.97	0.985	82.02
D_3	101.37	0.990	99.08	0.993	87.97	0.994	96.14
D_4	91.37	0.983	89.39	0.987	79.26	0.989	86.67
D_5	135.14	0.999	131.72	0.999	123.97	0.999	130.28
D_6	64.56	0.955	63.26	0.962	55.71	0.964	61.18
F_1	53.64	0.997	51.90	0.998	44.50	0.998	50.01
F_2	75.59	0.993	73.23	0.992	69.90	0.994	72.91
F_3	102.25	0.987	99.12	0.983	101.27	0.983	100.88
F_4	132.44	0.976	128.43	0.970	137.01	0.961	132.63
A_2	20.93	0.995	19.84	0.996	16.00	0.997	18.92
A_3	10.02	0.988	9.15	0.990	6.06	0.991	8.41
A_4	4.57	0.963	3.81	0.961	1.87	0.921	3.42
$A_{1/2}$	119.08	0.998	116.35	0.999	113.86	0.999	116.43
$A_{1/3}$	184.51	0.998	180.15	0.999	157.39	0.999	174.02
$A_{1/4}$	249.95	0.998	244.27	0.999	213.94	0.999	236.06
G_1	31.20	0.948	30.23	0.956	25.86	0.956	29.10
G_2	40.92	0.980	39.67	0.984	34.35	0.986	38.31
G_3	44.59	0.986	43.22	0.990	37.55	0.991	41.79
P_1	9.50	0.862	8.79	0.868	6.51	0.827	8.27
P_2	2.27	0.426	1.92	0.510	3.18	0.279	2.46
P_3	1.34	0.299	1.65	0.321	0.52	0.112	1.17

Table 10
The apparent activation energy acquired by the CR method for P-Lig.

Mechanism	10 K/min		20 K/min		30 K/min		Average (kJ/mol)
	$E\alpha$ (kJ/mol)	R^2	$E\alpha$ (kJ/mol)	R^2	$E\alpha$ (kJ/mol)	R^2	
D_1	94.67	0.981	108.95	0.993	88.80	0.990	97.47
D_2	110.13	0.990	122.80	0.995	105.60	0.991	112.84
D_3	130.10	0.996	139.73	0.995	127.57	0.987	132.46
D_4	116.69	0.993	128.39	0.995	112.81	0.990	119.30
D_5	176.12	0.995	177.46	0.990	178.51	0.985	177.37
D_6	82.07	0.975	96.06	0.982	75.80	0.989	84.64
F_1	69.13	0.996	85.77	0.99	67.13	0.977	74.01
F_2	103.86	0.981	129.32	0.971	111.01	0.946	114.73
F_3	146.56	0.960	182.99	0.949	166.21	0.919	165.25
F_4	195.13	0.943	244.11	0.933	228.94	0.902	222.73
A_2	27.51	0.995	35.58	0.987	26.07	0.965	29.72
A_3	13.63	0.992	18.85	0.981	12.39	0.938	14.96
A_4	6.70	0.984	10.48	0.969	5.55	0.854	7.58
$A_{1/2}$	152.38	0.997	186.14	0.992	149.24	0.981	162.59
$A_{1/3}$	235.62	0.997	286.53	0.992	231.35	0.982	251.17
$A_{1/4}$	318.86	0.997	386.90	0.992	313.46	0.982	339.74
G_1	43.34	0.987	53.58	0.991	36.54	0.986	44.49
G_2	55.14	0.996	68.27	0.994	50.21	0.987	57.87
G_3	59.55	0.997	73.79	0.994	55.48	0.984	62.94
P_1	14.62	0.969	19.49	0.983	10.78	0.961	14.96
P_2	5.04	0.883	8.12	0.956	2.20	0.695	5.12
P_3	0.25	0.129	2.44	0.768	2.10	0.779	1.60

CRediT authorship contribution statement

Jialiu Lei: Writing – review & editing, Writing – original draft, Methodology. **Liu Yang:** Data curation. **Yuhao Wang:** Investigation. **Dongnan Zhao:** Formal analysis, Conceptualization.

Data availability statement

Not applicable.

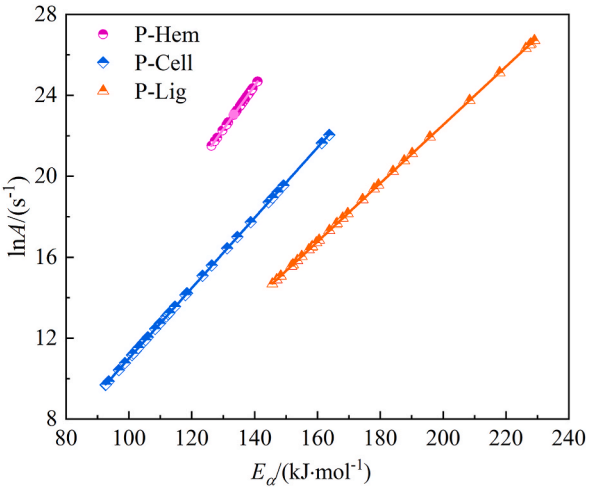

Fig. 9. The correlation between the activation energy and the pre-exponential factor.

Table 11
The kinetic compensation parameters for each P-Com.

Pseudo Components	*a*	*b*	R^2	MSN
P-Hem	0.216	5.818	1	0
P-Cell	0.173	6.376	0.9999	0.0002
P-Lig	0.144	6.318	0.9999	0.0001

Table 12
The thermodynamic parameters obtained by FWO, KAS, and Vyazoykin methods for P-Hem.

α	FWO				KAS				Vyazoykin			
	ln*A* (s^{-1})	Δ*H* (kJ/mol)	Δ*G* (kJ/mol)	Δ*S* (J/(mol × K))	ln*A* (s^{-1})	Δ*H* (kJ/mol)	Δ*G* (kJ/mol)	Δ*S* (J/(mol × K))	ln*A* (s^{-1})	Δ*H* (kJ/mol)	Δ*G* (kJ/mol)	Δ*S* (J/(mol × K))
0.10	24.69	136.59	166.96	−52.74	24.35	134.99	167.01	−55.61	23.86	132.73	167.09	−59.68
0.15	24.67	136.41	166.96	−53.06	24.29	134.64	167.02	−56.24	23.81	132.44	167.10	−60.20
0.20	23.91	132.85	167.08	−59.45	23.46	130.77	167.15	−63.19	23.48	130.83	167.15	−63.09
0.25	24.18	134.02	167.04	−57.35	23.72	131.89	167.11	−61.18	23.71	131.86	167.11	−61.23
0.30	24.10	133.62	167.05	−58.07	23.61	131.37	167.13	−62.11	23.49	130.80	167.15	−63.13
0.35	24.11	133.62	167.05	−58.07	23.60	131.28	167.13	−62.27	23.35	130.11	167.17	−64.38
0.40	24.02	133.16	167.06	−58.90	23.49	130.72	167.15	−63.28	23.45	130.53	167.15	−63.61
0.45	23.82	132.17	167.10	−60.66	23.26	129.58	167.19	−65.31	23.23	129.46	167.19	−65.54
0.50	23.80	132.04	167.10	−60.89	23.22	129.37	167.19	−65.69	23.08	128.73	167.22	−66.84
0.55	23.76	131.84	167.10	−61.25	23.16	129.07	167.20	−66.23	23.03	128.47	167.22	−67.31
0.60	23.70	131.50	167.11	−61.86	23.08	128.63	167.22	−67.02	23.25	129.46	167.19	−65.54
0.65	23.68	131.36	167.12	−62.11	23.03	128.40	167.22	−67.44	23.23	129.30	167.19	−65.82
0.70	23.75	131.66	167.11	−61.57	23.09	128.61	167.21	−67.05	23.70	131.43	167.11	−61.98
0.75	22.26	124.73	167.35	−74.03	21.50	121.22	167.48	−80.36	22.12	124.10	167.38	−75.17
0.80	22.67	126.54	167.28	−70.78	21.90	122.98	167.42	−77.19	22.62	126.31	167.29	−71.19
0.85	22.55	125.90	167.31	−71.92	21.73	122.15	167.44	−78.68	22.47	125.53	167.32	−72.58
Average	23.73	131.75	167.11	−61.42	23.16	129.10	167.20	−66.18	23.24	129.51	167.19	−65.46

Funding

Jialiu Lei was supported by by the Opening Foundation of The State Key Laboratory of Refractories and Metallurgy (Wuhan University of Science and Technology) (No. G202208), the Joint supported by Hubei Provincial Natural Science Foundation and Huangshi of China (No. 2023AFD010).

Declaration of competing interest

The authors declare that they have no known competing financial interests or personal relationships that could have appeared to influence the work reported in this paper.

Table 13
The thermodynamic parameters obtained by FWO, KAS, and Vyazoykin methods for P-Cell.

α	FWO				KAS				Vyazoykin			
	ln$A$ (s^{-1})	ΔH (kJ/mol)	ΔG (kJ/mol)	ΔS (J/(mol × K))	ln$A$ (s^{-1})	ΔH (kJ/mol)	ΔG (kJ/mol)	ΔS (J/(mol × K))	ln$A$ (s^{-1})	ΔH (kJ/mol)	ΔG (kJ/mol)	ΔS (J/(mol × K))
0.10	19.21	142.11	214.52	−99.72	18.72	139.29	214.64	−103.76	18.38	137.32	214.72	−106.58
0.15	22.04	158.38	213.88	−76.43	21.64	156.01	213.97	−79.82	21.21	153.56	214.06	−83.32
0.20	19.54	143.68	214.44	−97.44	18.94	140.22	214.58	−102.40	18.96	140.31	214.58	−102.28
0.25	17.74	133.13	214.88	−112.58	17.00	128.87	215.07	−118.71	17.07	129.25	215.05	−118.15
0.30	16.44	125.52	215.21	−123.52	15.60	120.66	215.44	−130.53	15.73	121.46	215.40	−129.37
0.35	15.09	117.64	215.58	−134.89	14.14	112.18	215.86	−142.78	14.27	112.94	215.82	−141.68
0.40	14.22	112.59	215.83	−142.18	13.19	106.68	216.14	−150.74	13.44	108.11	216.06	−148.67
0.45	13.56	108.69	216.03	−147.82	12.46	102.40	216.37	−156.95	12.73	103.97	216.28	−154.67
0.50	13.08	105.85	216.18	−151.93	11.92	99.24	216.54	−161.54	12.10	100.30	216.48	−160.00
0.55	12.73	103.78	216.29	−154.94	11.52	96.89	216.68	−164.97	11.73	98.06	216.61	−163.26
0.60	12.05	99.82	216.50	−160.69	10.77	92.55	216.93	−171.30	11.20	94.96	216.78	−167.76
0.65	11.76	98.06	216.60	−163.24	10.43	90.52	217.05	−174.25	10.88	93.09	216.89	−170.49
0.70	11.39	95.90	216.72	−166.38	13.25	106.53	216.12	−150.92	12.96	104.83	216.21	−153.39
0.75	11.29	95.20	216.75	−167.40	9.86	87.09	217.26	−179.26	10.62	91.38	216.99	−172.98
0.80	11.17	94.39	216.80	−168.58	9.69	85.98	217.32	−180.88	10.41	90.07	217.06	−174.88
0.85	11.25	94.70	216.77	−168.10	9.71	85.98	217.31	−180.85	10.45	90.19	217.04	−174.70
Average	14.54	114.34	215.81	−139.74	13.68	109.44	216.08	−146.85	13.88	110.61	216.00	−145.14

Table 14
The thermodynamic parameters obtained by FWO, KAS, and Vyazoykin methods for P-Lig.

α	FWO				KAS				Vyazoykin			
	ln$A$ (s^{-1})	ΔH (kJ/mol)	ΔG (kJ/mol)	ΔS (J/(mol × K))	ln$A$ (s^{-1})	ΔH (kJ/mol)	ΔG (kJ/mol)	ΔS (J/(mol × K))	ln$A$ (s^{-1})	ΔH (kJ/mol)	ΔG (kJ/mol)	ΔS (J/(mol × K))
0.10	26.32	221.27	256.54	−40.72	26.55	222.87	256.49	−38.82	25.83	217.79	256.65	−44.87
0.15	19.58	173.68	258.21	−97.61	20.76	181.87	257.89	−87.78	19.83	175.44	258.14	−95.50
0.20	23.75	202.07	257.13	−63.59	25.13	211.64	256.81	−52.16	24.44	206.86	256.97	−57.87
0.25	26.71	222.39	256.45	−39.33	26.50	220.89	256.50	−41.12	26.32	219.65	256.54	−42.60
0.30	18.84	167.55	258.42	−104.94	18.16	162.87	258.61	−110.57	18.23	163.33	258.59	−110.01
0.35	17.63	159.05	258.77	−115.16	16.85	153.66	259.01	−121.66	16.90	154.03	258.99	−121.21
0.40	16.50	151.20	259.12	−124.62	15.63	145.23	259.39	−131.83	15.82	146.49	259.34	−130.31
0.45	15.63	145.10	259.40	−131.98	14.68	138.63	259.71	−139.82	14.90	140.09	259.64	−138.05
0.50	15.84	146.50	259.33	−130.29	14.88	139.93	259.64	−138.24	14.97	140.52	259.61	−137.52
0.55	16.04	147.80	259.26	−128.72	15.07	141.14	259.58	−136.77	15.16	141.75	259.55	−136.03
0.60	16.53	151.07	259.11	−124.76	15.56	144.41	259.42	−132.81	15.88	146.63	259.31	−130.13
0.65	17.32	156.43	258.87	−118.30	16.37	149.88	259.16	−126.20	16.70	152.16	259.06	−123.44
0.70	17.67	158.80	258.76	−115.43	16.72	152.22	259.05	−123.37	17.43	157.09	258.83	−117.49
0.75	18.85	166.82	258.42	−105.78	17.93	160.49	258.68	−113.40	18.64	165.42	258.47	−107.46
0.80	20.25	176.41	258.03	−94.25	19.38	170.40	258.27	−101.47	20.02	174.82	258.09	−96.16
0.85	21.94	188.03	257.58	−80.32	21.13	182.39	257.79	−87.08	21.77	186.84	257.63	−81.74
Average	19.34	170.89	258.34	−100.99	18.83	167.41	258.50	−105.19	18.93	168.06	258.46	−104.40

Acknowledgments

The authors gratefully acknowledge the resources partially provided by the State Key Laboratory of Refractories & Metallurgy, Wuhan University of Science and Technology.

References

[1] A. Saravanakumar, P. Vijayakumar, A.T. Hoang, E.E. Kwon, W.H. Chen, Thermochemical conversion of large-size woody biomass for carbon neutrality: principles, applications, and issues, Bioresour. Technol. 370 (2023) 128562, https://doi.org/10.1016/j.biortech.2022.128562.
[2] M.X. Li, N.P. He, L. Xu, C.H. Peng, H. Chen, G.R. Yu, Eco-CCUS: a cost-effective pathway towards carbon neutrality in China, Renew. Sustain. Energy Rev. 183 (2023) 113512, https://doi.org/10.1016/j.rser.2023.113512.
[3] D. Ravelli, C. Samorì, Biomass Valorisation, Wiley-VCH, Weinheim, Germany, 2021.
[4] N. Tripathi, C.D. Hills, R.S. Singh, C.J. Atkinson, Biomass waste utilisation in low-carbon products: harnessing a major potential resource, NPJ Clim. Atmos. Sci. 2 (2019) 35–44, https://doi.org/10.1038/s41612-019-0093-5.
[5] Y. Nie, M. Deng, M. Shan, X. Yang, Evaluating the impact of wood sawdust and peanut shell mixing ratio on co-combustion performance, Fuel 324 (2022) 124667, https://doi.org/10.1016/j.fuel.2022.124667.
[6] J.A. Okolie, E.I. Epelle, M.E. Tabat, U. Orivri, A.N. Amenaghawon, P.U. Okoye, B. Gunes, Waste biomass valorization for the production of biofuels and value-added products: a comprehensive review of thermochemical, biological and integrated processes, Process Saf. Environ. 159 (2022) 323–344, https://doi.org/10.1016/j.psep.2021.12.049.
[7] A.M. Elgarahy, A. Hammad, D.M. El-Sherif, M. Abouzid, M.S. Gaballah, K.Z. Elwakeel, Thermochemical conversion strategies of biomass to biofuels, techno-economic and bibliometric analysis: a conceptual review, J. Environ. Chem. Eng. 9 (2021) 106503, https://doi.org/10.1016/j.jece.2021.106503.

[8] J.C. Solarte-Toro, J.A. González-Aguirre, J.A.P. Giraldo, C.A.C. Alzate, Thermochemical processing of woody biomass: a review focused on energy-driven applications and catalytic upgrading, Renew. Sustain. Energy Rev. 136 (2021) 110376, https://doi.org/10.1016/j.rser.2020.110376.

[9] L.Y. Qin, Y. Shao, Z.W. Hou, E.C. Jiang, Effect of temperature on the physicochemical characteristics of pine nut shell pyrolysis products in a screw reactor, Energy Source. Part A 42 (2020) 2831–2843, https://doi.org/10.1080/15567036.2019.1618993.

[10] Y.C. Li, B. Xing, Y. Ding, X.H. Han, S.R. Wang, A critical review of the production and advanced utilization of biochar via selective pyrolysis of lignocellulosic biomass, Bioresour. Technol. 312 (2020) 123614, https://doi.org/10.1016/j.biortech.2020.123614.

[11] N. Abdullah, R.M. Taib, N.S.M. Aziz, M.R. Omar, N.M. Disa, Banana pseudo-stem biochar derived from slow and fast pyrolysis process, Heliyon 9 (2023) e12940, https://doi.org/10.1016/j.heliyon.2023.e12940.

[12] G.Y. Wang, Y.J. Dai, H.P. Yang, Q.G. Xiong, K.G. Wang, J.S. Zhou, Y.C. Li, S.R. Wang, A review of recent advances in biomass pyrolysis, Energy Fuels 34 (2020) 15557–15578, https://doi.org/10.1021/acs.energyfuels.0c03107.

[13] R. Singh, B.B. Krishna, G. Mishra, J. Kumar, T. Bhaskar, Strategies for selection of thermo-chemical processes for the valorisation of biomass, Renew. Energy 98 (2016) 226–237, https://doi.org/10.1016/j.renene.2016.03.023.

[14] X. Zhang, H.H. Deng, X.Y. Hou, R.L. Qiu, Z.H. Chen, Pyrolytic behavior and kinetic of wood sawdust at isothermal and non-isothermal conditions, Renew. Energy 142 (2019) 284–294, https://doi.org/10.1016/j.renene.2019.04.115.

[15] M. Hussain, H. Zabiri, L.D. Tufa, S. Yusup, I. Ali, A kinetic study and thermal decomposition characteristics of palm kernel shell using model-fitting and model-free methods, Biofuels 13 (2022) 105–116, https://doi.org/10.1080/17597269.2019.1642642.

[16] I. Ali, S.R. Naqvi, A. Bahadar, Kinetic analysis of botryococcus braunii pyrolysis using model-free and model-fitting methods, Fuel 214 (2018) 369–380, https://doi.org/10.1016/j.fuel.2017.11.046.

[17] J. Kristanto, M.M. Azis, S. Purwono, Multi-distribution activation energy model on slow pyrolysis of cellulose and lignin in TGA/DSC, Heliyon 7 (2021) e07669, https://doi.org/10.1016/j.heliyon.2021.e07669.

[18] O. Fischer, R. Lemaire, A. Bensakhria, Thermogravimetric analysis and kinetic modeling of the pyrolysis of different biomass types by means of model-fitting, model-free and network modeling approaches, J. Therm. Anal. Calorim. (2024) 1–23, https://doi.org/10.1007/s10973-023-12868-w.

[19] P. Budrugeac, A. Cucos, R. Dascălu, I. Atkinson, P. Osiceanu, Application of model-free and multivariate nonlinear regression methods for evaluation of the kinetic scheme and kinetic parameters of thermal decomposition of low density polyethylene, Thermochim. Acta 708 (2022) 179138, https://doi.org/10.1016/j.tca.2021.179138.

[20] S. Vyazovkin, A.K. Burnham, L. Favergeon, N. Koga, E. Moukhina, L.A. P'erez-Maqueda, N. Sbirrazzuoli, ICTAC kinetics committee recommendations for analysis of multi-step kinetics, Thermochim. Acta 689 (2020) 178597, https://doi.org/10.1016/j.tca.2020.178597.

[21] W.M. Tao, P. Zhang, X.W. Yang, H. Li, Y. Liu, B. Pan, An integrated study on the pyrolysis mecanism of peanut shell based on the kinetic analysis and solid/gas characterization, Bioresour. Technol. 329 (2021) 124860, https://doi.org/10.1016/j.biortech.2021.124860.

[22] S. Singh, J.P. Chakraborty, M.K. Mondal, Intrinsic kinetics, thermodynamic parameters and reaction mechanism of nonisothermal degradation of torrefied acacia nilotica using isoconversional methods, Fuel 259 (2020) 116263, https://doi.org/10.1016/j.fuel.2019.116263.

[23] N. Sbirrazzuoli, Kinetic analysis of complex chemical reactions by coupling model-free and model-fitting analysis, Thermochim. Acta 719 (2023) 179416, https://doi.org/10.1016/j.tca.2022.179416.

[24] K. Li, W. Zhang, M.L. Fu, C.Z. Li, Z.L. Xue, Discussion on criterion of determination of the kinetic parameters of the linear heating reactions, Minerals 12 (2022) 81, https://doi.org/10.3390/min12010081.

[25] S.Y. Chen, J.M. Cai, Thermal decomposition kinetics of sweet sorghum bagasse analysed by model free methods, J. Energy Inst. 84 (2011) 1–4, https://doi.org/10.1179/014426010X12759937396759.

[26] S. Collins, P. Ghodke, Kinetic parameter evaluation of groundnut shell pyrolysis through use of thermogravimetric analysis, J. Environ. Chem. Eng. 6 (2018) 4736–4742, https://doi.org/10.1016/j.jece.2018.07.012.

[27] A. Bhavanam, R.C. Sastry, Kinetic study of solid waste pyrolysis using distributed activation energy model, Bioresour. Technol. 178 (2015) 126–131, https://doi.org/10.1016/j.biortech.2014.10.028.

[28] E. Torres-García, L.F. Ramírez-Verduzco, J. Aburto, Pyrolytic degradation of peanut shell: activation energy dependence on the conversion, Waste, Manag 106 (2020) 203–212, https://doi.org/10.1016/j.wasman.2020.03.021.

[29] A.K. Varma, S. Singh, A.K. Rathore, L.S. Thakur, R. Shankar, P. Mondal, Investigation of kinetic and thermodynamic parameters for pyrolysis of peanut shell using thermogravimetric analysis, Biomass Convers. Bior. 12 (2020) 4877–4888, https://doi.org/10.1007/s13399-020-00972-y.

[30] M. Kumar, D. Rai, G. Bhardwaj, S.N. Upadhyay, P.K. Mishra, Pyrolysis of peanut shell: kinetic analysis and optimization of thermal degradation process, Ind. Crop. Prod. 174 (2021) 114128, https://doi.org/10.1016/j.indcrop.2021.114128.

[31] T.T. Qu, W.J. Guo, L.H. Shen, J. Xiao, K. Zhao, Experimental study of biomass pyrolysis based on three major components: hemicellulose, cellulose, and lignin, Ind. Eng. Chem. Res. 50 (2011) 10424–10433, https://doi.org/10.1021/ie1025453.

[32] D.Y. Chen, K.H. Cen, X.Z. Zhuang, Z.Y. Gan, J.B. Zhou, Y.M. Zhang, H. Zhang, Insight into biomass pyrolysis mechanism based on cellulose, hemicellulose, and lignin: evolution of volatiles and kinetics, elucidation of reaction pathways, and characterization of gas, biochar and bio-oil, Combust. Flame 242 (2022) 112142, https://doi.org/10.1016/j.combustflame.2022.112142.

[33] F.X. Collard, J. Blin, A review on pyrolysis of biomass constituents: mechanisms and composition of the products obtained from the conversion of cellulose, hemicelluloses and lignin, Renew. Sustain. Energy Rev. 38 (2014) 594–608, https://doi.org/10.1016/j.rser.2014.06.013.

[34] Y. Wang, S.L. Yang, G.R. Bao, H. Wang, Investigation of tobacco straw pyrolysis: three-parallel Gaussian reaction modeling, products analysis and ANN application, Ind. Crop. Prod. 200 (2023) 116864, https://doi.org/10.1016/j.indcrop.2023.116864.

[35] R.Z. Huang, Z.Z. Teng, S. Li, Gaussian model analysis and thermal decomposition kinetics of nature fibers, J. Clean. Prod. 357 (2022) 131784, https://doi.org/10.1016/j.jclepro.2022.131784.

[36] B. Janković, N. Manić, D. Stojiljković, V. Jovanović, TSA-MS characterization and kinetic study of the pyrolysis process of various types of biomass based on the Gaussian multi-peak fitting and peak-to-peak approaches, Fuel 234 (2018) 447–463, https://doi.org/10.1016/j.fuel.2018.07.051.

[37] S. Guo, X.Y. Deng, L.D. Liu, L.Y. Ge, G. Lisak, Comprehensive analysis of combustion behavior, kinetics, and gas emissions of fungus bran biofuel through torrefaction pretreatment and polypropylene addition, Fuel 364 (2024) 131014, https://doi.org/10.1016/j.fuel.2024.131014.

[38] R.Y. Chen, Q.W. Li, Y. Zhang, X.K. Xu, D.D. Zhang, Pyrolysis kinetics and mechanism of typical industrial non-tyre rubber wastes by peak-differentiating analysis and multi kinetics methods, Fuel 235 (2019) 1224–1237, https://doi.org/10.1016/j.fuel.2018.08.121.

[39] M. Van de Velden, J. Baeyens, A. Brems, B. Janssens, R. Dewil, Fundamentals, kinetics and endothermicity of the biomass pyrolysis reaction, Renew. Energy 35 (2010) 232–242, https://doi.org/10.1016/j.renene.2009.04.019.

[40] A. Brems, J. Baeyens, J. Beerlandt, R. Dewil, Thermogravimetric pyrolysis of waste polyethylene-terephthalate and Polystyrene: a Critical assessment of kinetics modelling, Resour. Conserv. Recycl. 55 (2011) 772–781, https://doi.org/10.1016/j.resconrec.2011.03.003.

[41] J.D. Zhang, W.H. Ji, Y.P. Yuan, W. Nan, W.H. Yuan, Pyrolysis characteristics and kinetics study of four typical trolley case materials in passenger trains, Energy 292 (2024) 130548, https://doi.org/10.1016/j.energy.2024.130548.

[42] D.Y. Chen, K.H. Cen, X.Z. Zhuang, Z.Y. Gan, J.B. Zhou, Y.M. Zhang, H. Zhang, Insight into biomass pyrolysis mechanism based on cellulose, hemicellulose, and lignin: evolution of volatiles and kinetics, elucidation of reaction pathways, and characterization of gas, biochar and bio-oil, Combust. Flame 242 (2022) 112142, https://doi.org/10.1016/j.combustflame.2022.112142.

[43] A. Nawaz, P. Kumar, Elucidating the bioenergy potential of raw, hydrothermally carbonized and torrefied waste arundo donax biomass in terms of physicochemical characterization, kinetic and thermodynamic parameters, Renew. Energy 187 (2022) 844–856, https://doi.org/10.1016/j.renene.2022.01.102.

[44] E. Galiwango, M. Ismail, M.S. Ahmad, S. Al-Zuhair, Effect of thermo-responsive switchable solvents on microalgae cells' disruption and non-isothermal combustion kinetics, Biomass Conv. Bioref. 12 (2020) 3275–3288, https://doi.org/10.1007/s13399-020-00893-w.

[45] J.L.F. Alves, J.C.G. Da Silva, V.F. da Silva Filho, R.F. Alves, W.V. de Araujo Galdino, S.L.F. Andersen, R.F. De Sena, Determination of the bioenergy potential of Brazilian pine-fruit shell via pyrolysis kinetics, thermodynamic study, and evolved gas analysis, Bioenergy Res. 12 (2019) 168–183, https://doi.org/10.1007/s12155-019-9964-1.
[46] D. Rammohan, N. Kishore, R.V.S. Uppaluri, Insights on kinetic triplets and thermodynamic analysis of delonix regia biomass pyrolysis, Bioresour. Technol. 358 (2022) 127375, https://doi.org/10.1016/j.biortech.2022.127375.
[47] C.D. Doyle, Estimating isothermal life from thermogravimetric data, J. Appl. Polym. Sci. 6 (1962) 639–642, https://doi.org/10.1002/app.1962.070062406.
[48] J.H. Flynn, The "temperature integral"-its use and abuse, Thermochim. Acta 300 (1997) 83–92, https://doi.org/10.1016/S0040-6031(97)00046-4.
[49] T.A. Ozawa, A new method of analyzing thermogravimetric data, B. Chem. Soc. Jpn. 38 (1965) 1881–1886, https://doi.org/10.1246/bcsj.38.1881.
[50] K. Garba, I.Y. Mohammed, Y.M. Isa, L.G. Abubakar, Y.A. Abakr, B.H. Hameed, Pyrolysis of canarium schweinfurthii hard-shell: thermochemical characterisation and pyrolytic kinetics studies, Heliyon 9 (2023) e13234, https://doi.org/10.1016/j.heliyon.2023.e13234.
[51] A. Mianowski, M. Sciazko, T. Radko, Vyazovkin's isoconversional method as a universal approach, Thermochim. Acta 696 (2021) 178822, https://doi.org/10.1016/j.tca.2020.178822.
[52] K. Li, C. Gan, W. Zhang, C.Z. Li, G.Q. Li, Validity of isothermal kinetic prediction by advanced isoconversional method, Chem. Phys. 567 (2023) 111801, https://doi.org/10.1016/j.chemphys.2022.111801.
[53] S. Vyazovkin, Isoconversional Kinetics of Thermally Stimulated Processes, Springer, Berlin, Germany, 2015.
[54] G.I. Senum, R.T. Yang, Rational approximations of the integral of the Arrhenius function, J. Therm. Anal. 11 (1977) 445–447, https://doi.org/10.1007/BF01903696.
[55] A.W. Coats, J. Redfern, Kinetic parameters from thermogravimetric data, Nature 201 (1964) 68–69, https://doi.org/10.1038/201068a0.
[56] R.K. Singh, T. Patil, D. Pandey, S.P. Tekade, A.N. Sawarkar, Co-pyrolysis of petroleum coke and banana leaves biomass: kinetics, reaction mechanism, and thermodynamic analysis, J. Environ. Manage. 301 (2022) 113854, https://doi.org/10.1016/j.jenvman.2021.113854.
[57] V. Dhyani, J. Kumar, T. Bhaskar, Thermal decomposition kinetics of sorghum straw via thermogravimetric analysis, Bioresour. Technol. 245 (2017) 1122–1129, https://doi.org/10.1016/j.biortech.2017.08.189.
[58] R.Y. Chen, Q.W. Li, X.K. Xu, D.D. Zhang, Pyrolysis kinetics and reaction mechanism of representative non-charring polymer waste with micron particle size, Energy Convers. Manag. 198 (2019) 111923, https://doi.org/10.1016/j.enconman.2019.111923.
[59] R.Y. Chen, Q.W. Li, X.K. Xu, D.D. Zhang, R.L. Hao, Combustion characteristics, kinetics and thermodynamics of pinus sylvestris pine needle via non-isothermal thermogravimetry coupled with model-free and model-fitting methods, Case Stud. Therm. Eng. 22 (2020) 100756, https://doi.org/10.1016/j.csite.2020.100756.
[60] J.L.F. Alves, J.C.G. Da Silva, V.F. Da Silva Filho, R.F. Alves, M.S. Ahmad, W.V.A. Galdino, R.F. De Sena, Bioenergy potential of red macroalgae gelidium floridanum by pyrolysis: evaluation of kinetic triplet and thermodynamics parameters, Bioresour. Technol. 291 (2019) 121892, https://doi.org/10.1016/j.biortech.2019.121892.
[61] S. Vyazovkin, A.K. Burnham, J.M. Criado, L.A. Pérez-Maqueda, C. Popescu, N. Sbirrazzuoli, ICTAC kinetics committee recommendations for performing kinetic computations on thermal analysis data, Thermochim. Acta 520 (2011) 1–19, https://doi.org/10.1016/j.tca.2011.03.034.
[62] W.H. Chen, C.F. Eng, Y.Y. Lin, Q.V. Bach, Independent parallel pyrolysis kinetics of cellulose, hemicelluloses and lignin at various heating rates analyzed by evolutionary computation, Energy Convers. Manag. 221 (2020) 113165, https://doi.org/10.1016/j.enconman.2020.113165.
[63] P.J. Zong, Y. Jiang, Y.Y. Tian, J. Li, M. Yuan, Y.Y. Ji, M.S. Chen, D.W. Li, Y.Y. Qiao, Pyrolysis behavior and product distributions of biomass six group components: starch, cellulose, hemicellulose, lignin, protein and oil, Energy Convers. Manag. 216 (2020) 112777, https://doi.org/10.1016/j.enconman.2020.112777.
[64] R.H. Dong, F.J. Chen, F.X. Zhang, S.L. Yang, H.L. Liu, H. Wang, J.H. Hu, A comprehensive evaluation on pyrolysis kinetics, thermodynamics, product properties and formation pathways of jatropha oil for high-value utilization, Fuel 313 (2022) 122982, https://doi.org/10.1016/j.fuel.2021.122982.
[65] A. Tabal, A. Barakat, A. Aboulkas, K. El harfi, Pyrolysis of ficus nitida wood: determination of kinetic and thermodynamic parameters, Fuel 283 (2021) 119253, https://doi.org/10.1016/j.fuel.2020.119253.
[66] W.M. Tao, P. Zhang, X.W. Yang, H. Li, Y. Liu, B. Pan, An integrated study on the pyrolysis mecanism of peanut shell based on the kinetic analysis and solid/gas characterization, Bioresour. Technol. 329 (2021) 124860, https://doi.org/10.1016/j.biortech.2021.124860.
[67] Y. Qiao, B. Wang, Y. Ji, F. Xu, P. Zong, J. Zhang, Y. Tian, Thermal decomposition of castor oil, corn starch, soy protein, lignin, xylan, and cellulose during fast pyrolysis, Bioresour. Technol. 278 (2019) 287–295, https://doi.org/10.1016/j.biortech.2019.01.102.
[68] J. Parikh, S.A. Channiwala, G.K. Ghosal, A correlation for calculating HHV from proximate analysis of solid fuels, Fuel 84 (2005) 487–494, https://doi.org/10.1016/j.fuel.2004.10.010.
[69] J. LeBlanc, M. Uchimiya, G. Ramakrishnan, M.J. Castaldi, A. Orlov, Across-phase biomass pyrolysis stoichiometry, energy balance, and product formation kinetics, Energy Fuels 30 (2016) 6537–6546, https://doi.org/10.1021/acs.energyfuels.6b01376.
[70] K. Crombie, O. Mašek, Investigating the potential for a self-sustaining slow pyrolysis system under varying operating conditions, Bioresour. Technol. 162 (2014) 148–156, https://doi.org/10.1016/j.biortech.2014.03.134.